RESEARCH ARTICLE

Systematic and Differential Myelination of Axon Collaterals in the Mammalian Auditory Brainstem

Armin H. Seidl[1,2] and Edwin W Rubel[1,3]

A brainstem circuit for encoding the spatial location of sounds involves neurons in the cochlear nucleus that project to medial superior olivary (MSO) neurons on both sides of the brain via a single bifurcating axon. Neurons in MSO act as coincidence detectors, responding optimally when signals from the two ears arrive within a few microseconds. To achieve this, transmission of signals along the contralateral collateral must be faster than transmission of the same signals along the ipsilateral collateral. We demonstrate that this is achieved by differential regulation of myelination and axon caliber along the ipsilateral and contralateral branches of single axons; ipsilateral axon branches have shorter internode lengths and smaller caliber than contralateral branches. The myelination difference is established prior to the onset of hearing. We conclude that this differential myelination and axon caliber requires local interactions between axon collaterals and surrounding oligodendrocytes on the two sides of the brainstem.

GLIA 2016;64:487–494

Key words: differential myelination, conduction velocity, mammalian brainstem, precise timing

Introduction

The evolution of myelin in the vertebrate brain increased the speed at which neuronal information can be conveyed. Myelin also provides a mechanism to systematically and dynamically adjust conduction times of information flow between neuronal centers (Nave, 2010). While regulation of conduction time along axons is a common occurrence in the peripheral and central nervous system, its functional significance is not always clear (Kimura and Itami, 2009; Seidl, 2014). Recent studies in the avian auditory brainstem show how systematic regulation of conduction time is tied to a well-defined function in a neuronal circuit: Conduction times of binaurally elicited phase locked action potentials must be calibrated to ensure arrival within a small time window at the coincident detector neurons (Carr and Macleod, 2010; Ashida and Carr, 2011). We showed that variations in internode length and axon diameter are used to decrease the speed of signal propagation in the shorter axon branch relative to the longer axon branch (Seidl et al., 2010; Seidl et al., 2014). This conduction velocity regulation results in an equalization of conduction times with the required microsecond precision and enables the resolution of ITDs as small as 10 μs (Fischer and Seidl, 2014).

The mammalian sound localization circuit is comprised of coincidence detector neurons in the medial superior olive (MSO) that receive binaural excitatory inputs from neurons in the anteroventral cochlear nucleus (AVCN; Fig. 1A). Individual AVCN neuron axons bifurcate to send one collateral to the ipsilateral MSO and a second collateral to the contralateral MSO. Conduction velocity must be precisely timed to shift the best response of MSO cells into the physiological range of ITDs (Brand et al., 2002, Fig. 3c,d, when inhibition is blocked best ITDs based on excitation alone shift to 0 ITD; van der Heijden et al., 2013, Fig. 3B; Franken et al., 2015, Fig. 2e, most best ITDs are around 0 ITD). Because the hearing range of the Mongolian Gerbil is similar to humans, it has become an important laboratory animal for studies on sound localization. The physiological range of ITDS in gerbils (the range of naturally occurring ITDs) is ±110-135 μs (Maki and Furukawa, 2005; see also

View this article online at wileyonlinelibrary.com. DOI: 10.1002/glia.22941

Published online November 10, 2015 in Wiley Online Library (wileyonlinelibrary.com). Received July 13, 2015, Accepted for publication Oct 20, 2015.

Address correspondence to Armin H. Seidl, Virginia Merrill Bloedel Hearing Research Center, University of Washington, Box 357923, Seattle, WA 98195-7923. E-mail: armins@uw.edu

From the [1]Virginia Merrill Bloedel Hearing Research Center, University of Washington, Seattle, Washington; [2]Department of Neurology, University of Washington, Seattle, Washington; [3]Department of Otolaryngology – Head & Neck Surgery, University of Washington, Seattle, Washington

Additional Supporting Information may be found in the online version of this article.

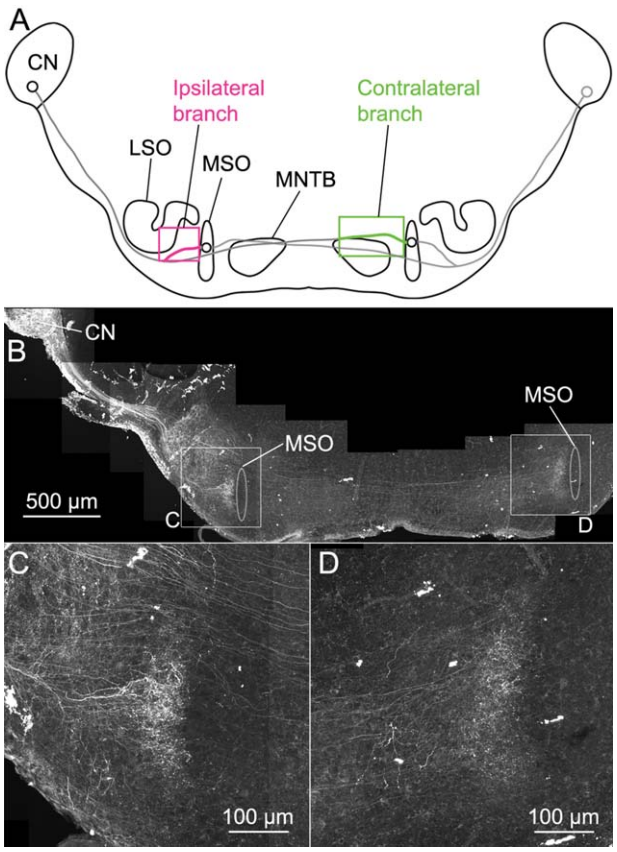

FIGURE 1: Mammalian ITD circuit. A: Anteroventral cochlear nucleus (AVCN) axons bifurcate and their excitatory collaterals project to the ipsilateral and contralateral MSO. Each MSO neuron gets binaural inputs mediated by AVCN neurons from both sides. Magenta and green square outlines show approximate locations of labeled fibers used for analysis. B: Labeled AVCN axons project ventrally and to the contralateral side, branching off to project to the ipsilateral MSO, before continuing to the contralateral MSO [dotted oval outlines denote position of MSO somata, dendrites can extend up to 140 µm to each side (Kapfer et al., 2002)]. The contralateral axon branch can approach 4 mm in length (data not shown). C,D. Closeup of ipsilateral and contralateral axon terminal areas as indicated by square outlines in (B).

Sterbing et al., 2003). The locations of the MSO nuclei interject a length disparity between the ipsi- and contralateral inputs, creating a major challenge for coincident input of action potential timing from the two ears (Stotler, 1953). We therefore hypothesized that axon diameters and internode lengths differ between ipsilateral and contralateral axons to adjust conduction times along the axonal inputs to provide coincident inputs to MSO neurons at naturally occurring ITDs.

We analyzed internode length and axon diameter in ipsilateral and contralateral branches of the AVCN axons projecting to MSO of the gerbil. Our data suggest that differential myelination and variations in axon diameter in two different branches of individual axon collaterals are a shared principle in the auditory systems of birds and mammals, and are utilized to achieve binaural coincident inputs in the microsecond range.

Materials and Methods

Animals

We used 44 gerbils (*Meriones unguiculatus*) of either sex, purchased from Charles River Laboratories (Wilmington, MA). Animals were used on the day of delivery to the University of Washington. All procedures were approved by the University of Washington Institutional Animal Care and Use Committee and conformed to National Institutes of Health guidelines.

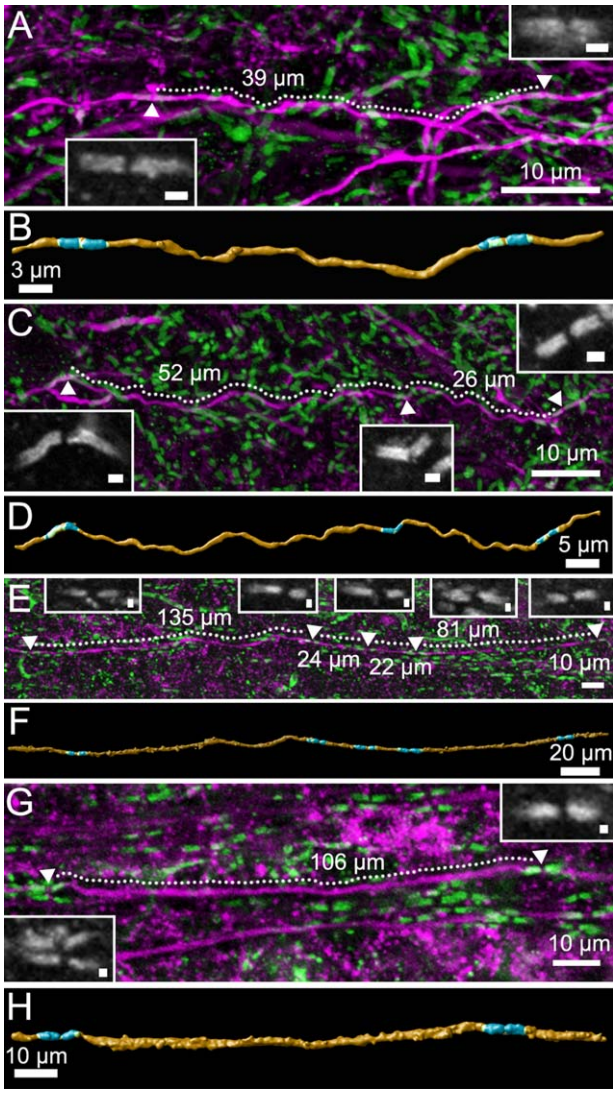

FIGURE 2: Internode length measurements along AVCN axons. Projection images of 3D image stacks containing labeled axons (magenta) and paranodes (green) of a P20 gerbil. Labeled axons are counterstained with antibodies against Caspr, a paranodal anchoring protein. Ipsilateral (A, C), contralateral (E, G) and their corresponding 3D reconstructions (ipsilateral: B, D; contralateral: F, H) allow the identification of axons and their labeled nodes of Ranvier (Axon: orange, paranodes: blue). Dotted lines in A,C, E, and G indicate axon segments along which the distance between two adjacent nodes of Ranvier was measured in 3D. Insets show Caspr labeling of respective nodes. Note the two short internodes in C. Scale bars in insets are 1 µm.

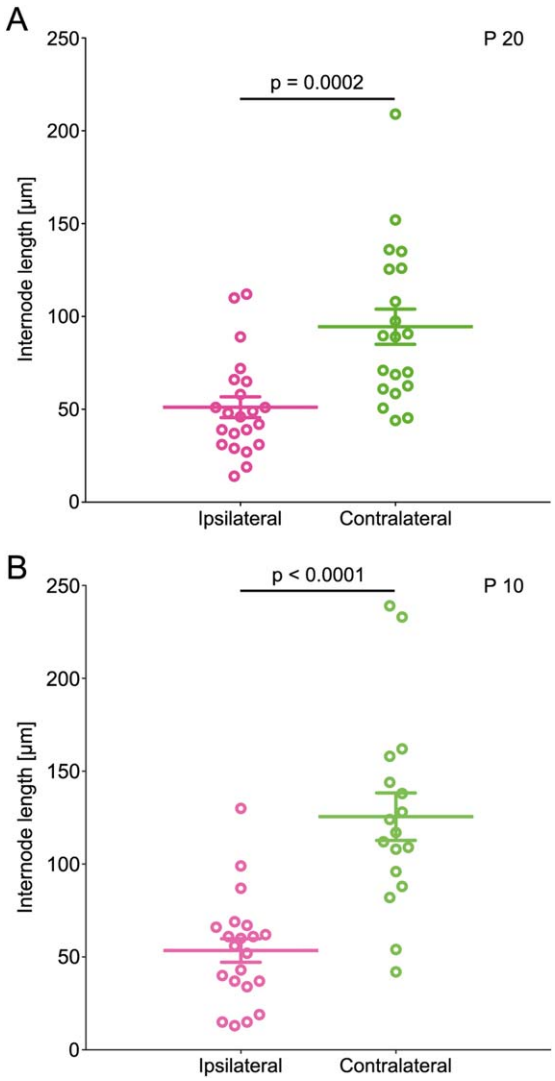

FIGURE 3: Differential internode length in AVCN axon. A: At P20 internode length is shorter in the ipsilateral AVCN axon than in the contralateral branch. B: Internode length is shorter in the ipsilateral AVCN axon branch compared to its contralateral counterpart at P10, 2 days before hearing onset.

Biocytin Application, Axon Labeling, and Caspr Staining

Animals were anesthetized with isoflurane, decapitated and the brain was extracted from the skull. After extraction, a biocytin crystal (Sigma-Aldrich, St. Louis, MO) was placed onto AVCN on one side and the brain was returned to oxygenated ACSF (Mathews et al., 2010). Following 2-4 h incubation at room temperature (RT), the brain was immersion fixed in 4% paraformaldehyde for 12 h at 4°C. Longer incubation times resulted in tissue deterioration and were avoided. Incubation times were sufficient to label contralateral axons up to 4 mm. After rinsing in phosphate-buffered saline (PBS), the brainstem was coronally sectioned at 75 µm on a vibratome. The resulting sections were counterstained with fluorescent streptavidin (1 : 1,000 Alexa Fluor® 568 or 594, Molecular Probes, Grand Island, NY) and an antibody against the paranodal protein Caspr (1 : 1,000, NeuroMab clone K65/35, NeuroMab, University of California, Davis, Davis CA) in a standard block solution (0.3% Triton X-100 (Sigma-Aldrich), 5% normal goat serum) for at least 6 h at RT or overnight at 4°C. The sections were then rinsed in PBS and exposed to a secondary antibody (1:200, Alexa Fluor 488 goat anti-mouse, Molecular Probes) in block solution overnight at 4°C. After a final rinse in PBS, the sections were coverslipped with Glycergel (Dako, Carpinteria, CA).

3D Internode Length Measurement

Animals in which biocytin placements successfully labeled axon collaterals were included in the data analysis (P10: 5; P20: 5). Sections containing both labeled AVCN to MSO axons and paranodal staining were imaged using a confocal microscope (Fluoview 1000, Olympus, 20x air lens, NA 0.75, Center Valley, PA, or Leica TCS SP8, 20x air lens, NA 0.75 and 60x water, NA 1.4, Leica, Buffalo Grove, IL) and internode length was measured in 3-D as described in Seidl et al. (2010). In most cases we made 2 to 4 individual measurements in a single axon; these were averaged to provide a single measurement for that segment. All well-filled axons that could be isolated from adjacent axons were included in our analyses.

Axon Diameter Measurement

We determined the diameter of axon segments in which internode length was measured. Optical sections were imported to Fiji software (National Institutes of Health, Bethesda, MD) and the full width at half maximum of individual axons segments was determined using the FWHM plugin (John Yew Soon Lim, Institute of Molecular Biology, National University of Singapore). Diameter was measured in between nodes of Ranvier of axons segments used for analysis of data in Fig. 3 and average diameter values of two to four individual measurements in a single axon were used for analysis. A recent study measuring axon diameter of spherical bushy axons extending contralaterally to MSO in the gerbil shows similar values for axon diameter as we report, validating our measurements of the contralateral axon (Ford et al., 2015; Fig. 1e). In a previous study we validated axon diameter measurements with electron microscopy and found no significant difference between the groups (Seidl et al., 2010).

3D Reconstruction

Images in Fig. 2B,D,F,H were surface-rendered with Huygens Essential (Scientific Volume Imaging, Hilversum, The Netherlands).

Data Analysis

Statistical analyses and graphs were created using Prism (GraphPad Software, La Jolla, CA). Differences between groups were tested with an unpaired *t* test. All in-text and graphic representations of data illustrate the mean ± standard error of the mean. We performed a linear regression analysis and computed Pearson Product Moment correlations for the data presented in Figure 4 B and D.

Results

We analyzed internode length in AVCN axons of 22 ipsilateral axon branches and 20 contralateral axon branches from 5 P20 gerbils. Individual measurements in a single axon were averaged to provide a single measurement for that collateral. The exact

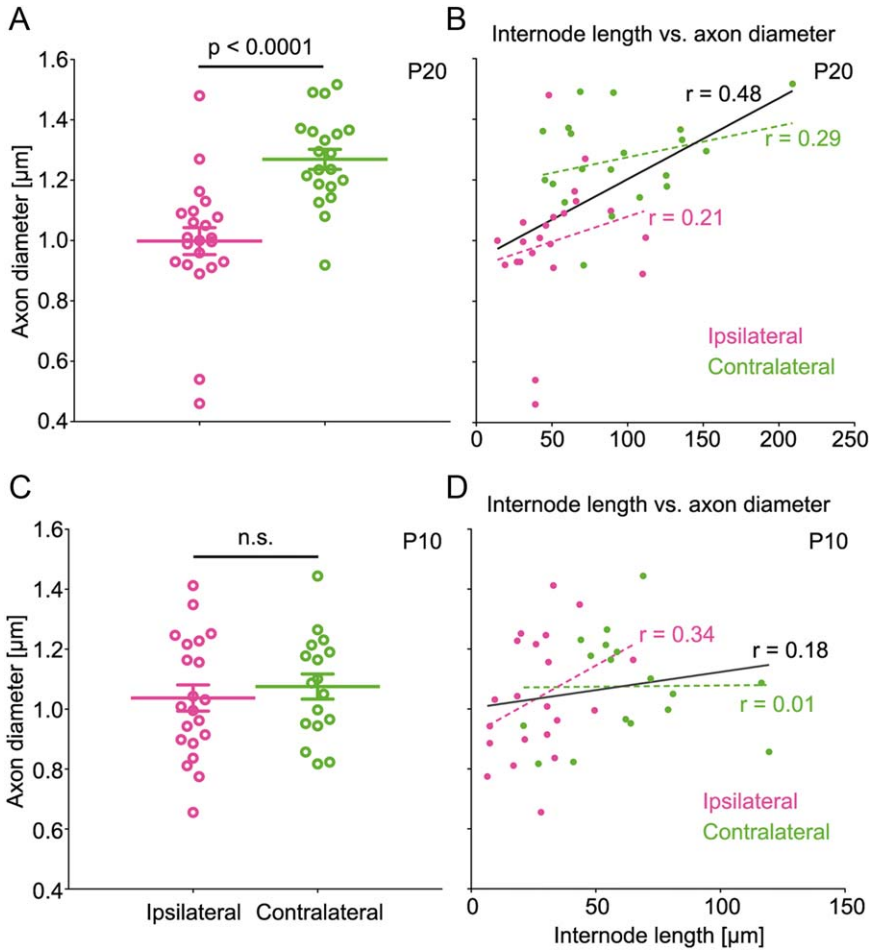

FIGURE 4: Axon diameter of axon segments. A: Average axon diameter of axon segments used for analysis in Fig. 3A. At P20 axon diameter in contralateral axon branches is larger than in the ipsilateral axon branches. B: Axon diameters of ipsilateral (magenta) and contralateral (green) axon segments combined are correlated to internode length at P20 (black line). C: Average axon diameter of axon segments used for analysis in Fig. 3C. Axon diameters of ipsilateral and contralateral axon branches are not different at P10. D: At P10, axon diameters of ipsilateral (magenta) and contralateral (green) axon segments are not correlated to internode length (black line).

location of the branch point initiating the ipsilateral and contralateral axons is not as evident in the gerbil as in the chicken brainstem. For this reason labeled axon collaterals for analysis were identified by their location proximal to the respective MSO and the fact that they either terminated in the MSO dendrite region or displayed repeated branching, identifying them as terminal arbors (Fig. 1B–D). Internode length measurements were taken proximal to where the axons entered the dendritic area of MSO. Figure 2 shows representative examples of labeled ipsilateral (A,C) and contralateral (E,G) axon collaterals (magenta) that were counterstained with an antibody against the paranodal anchoring protein Caspr (green). Corresponding 3D reconstructions of the axon segments in Fig. 2 confirm the integrity of the labeled fibers and the location of the paranodes (Fig. 2B,D (ipsilateral) and F,H (contralateral)). Animated versions of Fig. 2B,D,F & H are available in the online version of the paper. At P20, average internode length in the ipsilateral axon was 51 ± 6 µm, (SEM). The average internode length in the contralateral axon collaterals was 95 ± 9 µm (Fig. 3A). Internode length was thus 1.85 times longer in the contralateral axon compared to the ipsilateral axon ($P = 0.0002$).

At P10, 2 days before hearing onset (Woolf and Ryan, 1984), the difference in internode length was already established. We determined internode length in 20 ipsilateral axon collaterals and 17 contralateral axon collaterals from 5 P10 gerbils (Fig. 3B). Average internode length for the ipsilateral axon collaterals was 54 ± 6 µm and 126 ± 13 µm for the contralateral axon collaterals. The distance between nodes of Ranvier in the contralateral axon branch was thus 2.3 times the value of the ipsilateral branch ($P < 0.0001$).

To further examine the development of axon parameters that are known to influence conduction velocity, we analyzed axon diameter of the axon segments in which internode length was determined. Fiber diameter was measured between nodes of Ranvier identified on axon segments used for analysis for data

in Fig. 3 and average values were used for analysis. At P20, axon diameter was larger in the contralateral axon segments (1.27 ± 0.03 μm, $n = 20$) compared to the ipsilateral axon segments (1.00 ± 0.04 μm, $n = 22$, $P < 0.0001$, Fig. 4A). Axon diameter measurements are correlated to corresponding internode length values at P20 (Fig. 4B, Pearson $r = 0.4805$). At P10, we calculated average axon diameter to be 1.04 ± 0.04 μm ($n = 21$) in the ipsilateral and 1.08 ± 0.04 μm ($n = 17$) in the contralateral axon segments (Fig. 4C). There was no correlation of individual axon diameter values with corresponding internode length at P10 (Fig 4D, Pearson $r = 0.1765$).

Discussion

In gerbils that have mature hearing capability we show that internode length is shorter in the ipsilateral axon branch compared to the contralateral branch of AVCN axons that project to MSO. In addition, axon diameter is increased in the contralateral axon segment compared to its ipsilateral counterpart. This finding implies that conduction velocity is regulated differentially in the two collaterals to compensate for the longer travel distance of the contralateral input to MSO. Anatomical restrictions are thus counterbalanced by variations of internode length and axon diameter, and the resulting change in conduction velocity. This difference in internode length is already established at P10, 2 days before the onset of hearing, but the maturation of differential axon diameter appears to lag. Our findings mirror an earlier study on internode length and axon diameter differences in the avian ITD processing circuit (Seidl et al., 2010), leading to an equalization of conduction times (Seidl et al., 2014). Combined, our studies suggest that differential myelination and differences in axon diameter along individual segments of a single axon form a general mechanism to regulate conduction time in the brainstem auditory pathways.

We measured fiber trajectories of labeled axons in 7 sections of 5 different animals. Pathway measurements are a good estimate of axon length (Seidl et al., 2010). Average pathway length from the ipsilateral AVCN to MSO was 1403 ± 771 μm and from the contralateral AVCN to MSO was 3541 ± 380 μm, resulting in an average difference of input length of 2138 ± 102 μm ($n = 7$). If action potentials were conducted with uniform speed along the AVCN axon, binaural inputs to MSO would differ by $267 - 1{,}069$ μs (based on conduction velocities ranging from 8 to 2 m/s). Internode length is a major determinant of conduction velocity (Brill et al., 1977) and axon branches of the analogous circuitry in the bird exhibit a 1.95-fold difference in internode length (Seidl et al., 2010), which translates to a 2.39-fold difference in conduction velocity (Seidl et al., 2014). In the gerbil, internode lengths of AVCN axon branches differ by a factor of 1.85. This difference in internode length can thus compensate for the longer contralateral input length, especially if one considers that internode length is one of several properties regulating action potential conduction velocity.

The avian ITD detection circuit embodies a modified Jeffress model (Carr and Konishi, 1990; Young and Rubel, 1983; Overholt et al., 1992; Köppl and Carr, 2008; Seidl et al., 2010). In contrast, the exact mechanisms of ITD coding in the mammalian auditory brainstem are still being resolved. Originally, MSO and its incoming projections were also considered to compose a circuit working according to the Jeffress place theory of sound localization (Yin and Chan, 1990; Smith et al., 1993; Beckius et al., 1999). *In vivo* recordings in the gerbil and guinea pig, however, show that best ITDs are not distributed across the range of naturally occurring ITDs, but support a population based rate code (McAlpine et al., 2001; Brand et al., 2002; Seidl and Grothe, 2005). In addition to their excitatory inputs, MSO neurons receive prominent glycinergic inhibition (Grothe and Sanes, 1993; Grothe and Sanes, 1994). These inhibitory inputs to MSO are anatomically and physiologically specialized for temporally precise synaptic transmission (Kapfer et al., 2002; Magnusson et al., 2005; Werthat et al., 2008; Couchman et al., 2010) and appear to play a role in the tuning of ITDs (Brand et al., 2002; Myoga et al., 2014; Pecka et al., 2008). The exact role of this inhibition is disputed. Other studies suggest ITD tuning is determined by the relative timing of binaural excitation to MSO (Day and Semple, 2011; van der Heijden et al., 2013; Roberts et al., 2013) and argue against a role of inhibition in ITD tuning (Franken et al., 2015). Regardless of the role of inhibition, however, precisely timed binaural excitation is mandatory for MSO function according to all proposed mechanisms. Our study supports the notion that conduction time of binaural excitatory projections to MSO is precisely regulated. As such, anatomical restrictions are overcome by variations in internode length and fiber diameter. Recent studies by Roberts and colleagues used an elegant *in vitro* preparation to show that excitatory input delays to MSO do not differ (Roberts et al., 2013), and thus support our conclusions of temporal compensation of inputs. Our data do not allow any conclusions about the role of inhibition in ITD coding. On the other hand, internode length along axons projecting to the medial nucleus of the trapezoid body (MNTB), which in turn provides an inhibitory input to MSO, appears to be specialized for fast signal transmission (Ford et al., 2015), supporting the concept of temporally precise glycinergic inhibition of MSO neurons (Kapfer et al., 2002).

Variations in myelination of axons are a common occurrence in the central nervous system (e.g., Bennett, 1970; Lang and Rosenbluth, 2003; Salami et al., 2003; Sugihara et al., 1993; Tomassy et al., 2014; Waxman, 1971; for review see Kimura and Itami, 2009; Seidl, 2014; de Hoz and Simons, 2015), yet the functional implications of this variability are not always clear.

The ITD detection networks of birds and mammals provide a unique preparation in which the normal function of this network can only be realized when the timing of action potentials emanating from the two ears are regulated in the microsecond range. Therefore, the selection pressure to modulate conduction times is clear and serves a well-defined computational function. We find that contralateral fibers display interspersed short internodes whose length is only a fraction of a regular internode. This is not without precedence, as short internodes have been described before (Waxman, 1971; Waxman and Melker, 1971). Variations in the geometry of the myelin sheath may provide a mechanism for temporal adjustment or more complex transformations of neural information in axons. It seems possible that short internodes are introduced for fine tuning conduction times to achieve specifically timed inputs to MSO.

Axon diameter in the contralateral axon segments is on average larger than in the ipsilateral segments at P20. This suggests that fiber caliber contributes to an increase in signal transmission speed in the contralateral axon branch projecting to MSO. However, axon diameter does not differ between the two axon branches at P10. Therefore, it appears that the intraaxonal difference in internode length, already established at P10, precedes differentiation in axon diameter.

Node of Ranvier assembly, node spacing, and axon diameter are controlled by myelinating glia (de Waegh et al., 1992; Court et al., 2004; Garcia et al., 2003; Susuki and Rasband, 2008). Studies of mature systems indicate that axon diameter and internode length in the peripheral nervous system are highly correlated (e.g., Hess and Young, 1949; Vizoso and Young, 1948; for review see Waxman, 1975). Our data support a significant correlation between these parameters in individual axons at P20. Both axon diameter and internode length are increased in the contralateral axon segments relative to the ipsilateral segments. Surprisingly, there appears to be no overall difference in axon caliber between the collaterals and the correlations between parameters do not approach significance at P10. This suggests that internodal length and axon caliber can be independently regulated.

We have now described data in homologous pathways in two divergent species indicating that separate collaterals of individual parent axons precisely regulate the interactions with surrounding neural elements to achieve markedly different conduction velocities. This results in precise integration of the timing of information from different sources to the postsynaptic neurons. While the resulting functional attributes are obvious for the processing of binaural acoustic information, the fundamental principal described in these papers has importance for understanding the temporal integration of signals required for all sensory information coding and motor coordination, particularly fine motor skills. Our data and interpretations thereby warrant some speculations about how the precise regulation of action potential velocity in these separate collaterals of the same parent axons is maintained and how it emerges during ontogeny, a period of substantial brain growth (Wilkinson, 1986). The ipsi- and contralateral axon collaterals of individual AVCN neurons are spatially separated within the brainstem. Differentially expressed genes along the pathways of the ipsilateral and contralateral trajectories could lead to differences in molecules in axons or in oligodendrocytes specifying the differences in internode length. To date no such molecule has been identified. There are multiple lines of evidence to indicate that excitatory neuronal activity instructs myelination (Barres and Raff, 1993; Bergles et al., 2000; Demerens et al., 1996; Fannon et al., 2015; Gibson et al., 2014; Goldsberry et al., 2011; Ishibashi et al., 2006; Káradóttir et al., 2005; Li et al., 2010; Lin et al., 2005; Mangin et al., 2008; Stevens et al., 1998; Ziskin et al., 2007). Specifically, electrically active axons can induce myelin formation by vesicular release of glutamate that signals NMDA receptors (NMDAR) on nearby OLs (Wake et al., 2011). Neuregulin (NRG1) appears to increase NMDAR currents in oligodendrocytes 6-fold (Lundgaard et al., 2013). Thus, specific NRG1-expression could enhance the sensitivity of oligodendrocytes to electrical activity from axons, caused by spontaneous activity before hearing onset (Jones et al., 2007; Walsh and McGee, 1988), and thus influence myelination. It has been demonstrated that different axons myelinated by a single oligodendrocyte can have myelin sheaths of different thicknesses, with myelin thickness dictated by the axon (Waxman and Sims, 1984). Other factors, such as Wnt (Guo et al., 2015), may influence myelination and internode length regulation as well. Future studies are needed to unravel the mechanisms of conduction velocity regulation and we think the auditory brainstem can serve as a useful tool to study how internode length is regulated, particularly in conjunction with transgenic mouse models (Pfrieger and Slezak, 2012).

Acknowledgment

Grant sponsors: Virginia Merrill Bloedel Hearing Research Center, the Hearing Health Foundation; Grant sponsor: NIH; Grant numbers: DC011343 (A.H.S.), DC003829, DC004661 (E.W. S.).

The authors thank David J. Perkel for comments on the manuscript.

References

Ashida G, Carr CE. 2011. Sound localization: Jeffress and beyond. Curr Opin Neurobiol 21:745–751.

Barres BA, Raff MC. 1993. Proliferation of oligodendrocyte precursor cells depends on electrical activity in axons. Nature 361:258–260.

Beckius GE, Batra R, Oliver DL. 1999. Axons from anteroventral cochlear nucleus that terminate in medial superior olive of cat: Observations related to delay lines. J Neurosci 19:3146–3161.

Bennett MV. 1970. Comparative physiology: Electric organs. Annu Rev Physiol 32:471–528.

Bergles DE, Roberts JD, Somogyi P, Jahr CE. 2000. Glutamatergic synapses on oligodendrocyte precursor cells in the hippocampus. Nature 405:187–191.

Brand A, Behrend O, Marquardt T, McAlpine D, Grothe B. 2002. Precise inhibition is essential for microsecond interaural time difference coding. Nature 417:543–547.

Brill MH, Waxman SG, Moore JW, Joyner RW. 1977. Conduction velocity and spike configuration in myelinated fibres: Computed dependence on internode distance. J Neurol Neurosurg Psychiatry 40:769–774.

Carr CE, Konishi M. 1990. A circuit for detection of interaural time differences in the brain stem of the barn owl. J Neurosci 10:3227–3246.

Carr CE, Macleod KM. 2010. Microseconds matter. PLoS Biol 8:e1000405-

Couchman K, Grothe B, Felmy F. 2010. Medial superior olivary neurons receive surprisingly few excitatory and inhibitory inputs with balanced strength and short-term dynamics. J Neurosci 30:17111–17121.

Court FA, Sherman DL, Pratt T, Garry EM, Ribchester RR, Cottrell DF, Fleetwood-Walker SM, Brophy PJ. 2004. Restricted growth of Schwann cells lacking Cajal bands slows conduction in myelinated nerves. Nature 431:191–195.

Day ML, Semple MN. 2011. Frequency-dependent interaural delays in the medial superior olive: implications for interaural cochlear delays. J Neurophysiol 106:1985–1999.

de Hoz L, Simons M. 2015. The emerging functions of oligodendrocytes in regulating neuronal network behaviour. Bioessays 37:60–69.

Demerens C, Stankoff B, Logak M, Anglade P, Allinquant B, Couraud F, Zalc B, Lubetzki C. 1996. Induction of myelination in the central nervous system by electrical activity. Proc Natl Acad Sci USA 93:9887–9892.

Fannon J, Tarmier W, Fulton D. 2015. Neuronal activity and AMPA-type glutamate receptor activation regulates the morphological development of oligodendrocyte precursor cells. Glia 63:1021–1035.

Fischer BJ, Seidl AH. 2014. Resolution of interaural time differences in the avian sound localization circuit–A modeling study. Front Comput Neurosci 8.

Ford MC, Alexandrova O, Cossell L, Stange-Marten A, Sinclair J, Kopp-Scheinpflug C, Pecka M, Attwell D, Grothe B. 2015. Tuning of Ranvier node and internode properties in myelinated axons to adjust action potential timing. Nat Commun 6:8073.

Franken TP, Roberts MT, Wei L, Golding NL, Joris PX. 2015. In vivo coincidence detection in mammalian sound localization generates phase delays. Nat Neurosci 18:444–452.

Garcia ML, Lobsiger CS, Shah SB, Deerinck TJ, Crum J, Young D, Ward CM, Crawford TO, Gotow T, Uchiyama Y, Ellisman MH, Calcutt NA, Cleveland DW. 2003. NF-M is an essential target for the myelin-directed "outside-in" signaling cascade that mediates radial axonal growth. J Cell Biol 163:1011–1020.

Gibson EM, Purger D, Mount CW, Goldstein AK, Lin GL, Wood LS, Inema I, Miller SE, Bieri G, Zuchero JB, Barres BA, Woo PJ, Vogel H, Monje M. 2014. Neuronal activity promotes oligodendrogenesis and adaptive myelination in the mammalian brain. Science 344:1252304.

Goldsberry G, Mitra D, MacDonald D, Patay Z. 2011. Accelerated myelination with motor system involvement in a neonate with immediate postnatal onset of seizures and hemimegalencephaly. Epilepsy Behav 22:391–394.

Grothe B, Sanes DH. 1993. Bilateral inhibition by glycinergic afferents in the medial superior olive. J Neurophysiol 69:1192–1196.

Grothe B, Sanes DH. 1994. Synaptic inhibition influences the temporal coding properties of medial superior olivary neurons: An in vitro study. J Neurosci 14:1701–1709.

Guo F, Lang J, Sohn J, Hammond E, Chang M, Pleasure D. 2015. Canonical Wnt signaling in the oligodendroglial lineage-puzzles remain. Glia 63:1671–1693.

Hess A, Young JZ. 1949. Correlation of internodal length and fibre diameter in the central nervous system. Nature 164:490.

Ishibashi T, Dakin KA, Stevens B, Lee PR, Kozlov SV, Stewart CL, Fields RD. 2006. Astrocytes promote myelination in response to electrical impulses. Neuron 49:823–832.

Jones TA, Leake PA, Snyder RL, Stakhovskaya O, Bonham B. 2007. Spontaneous discharge patterns in cochlear spiral ganglion cells before the onset of hearing in cats. J Neurophysiol 98:1898–1908.

Kapfer C, Seidl AH, Schweizer H, Grothe B. 2002. Experience-dependent refinement of inhibitory inputs to auditory coincidence-detector neurons. Nat Neurosci 5:247–253.

Káradóttir R, Cavelier P, Bergersen LH, Attwell D. 2005. NMDA receptors are expressed in oligodendrocytes and activated in ischaemia. Nature 438:1162–1166.

Kimura F, Itami C. 2009. Myelination and isochronicity in neural networks. Front Neuroanat 3:12.

Köppl C, Carr CE. 2008. Maps of interaural time difference in the chicken's brainstem nucleus laminaris. Biol Cybern 98:541–559.

Lang EJ, Rosenbluth J. 2003. Role of myelination in the development of a uniform olivocerebellar conduction time. J Neurophysiol 89:2259–2270.

Lin SC, Huck JH, Roberts JD, Macklin WB, Somogyi P, Bergles DE. 2005. Climbing fiber innervation of NG2-expressing glia in the mammalian cerebellum. Neuron 46:773–785.

Li Q, Brus-Ramer M, Martin JH, McDonald JW. 2010. Electrical stimulation of the medullary pyramid promotes proliferation and differentiation of oligodendrocyte progenitor cells in the corticospinal tract of the adult rat. Neurosci Lett 479:128–133.

Lundgaard I, Luzhynskaya A, Stockley JH, Wang Z, Evans KA, Swire M, Volbracht K, Gautier HO, Franklin RJ, Attwell D, Káradóttir RT. 2013. Neuregulin and BDNF induce a switch to NMDA receptor-dependent myelination by oligodendrocytes. PLoS Biol 11:e1001743.

Magnusson AK, Kapfer C, Grothe B, Koch U. 2005. Maturation of glycinergic inhibition in the gerbil medial superior olive after hearing onset. J Physiol 568:497–512.

Maki K, Furukawa S. 2005. Acoustical cues for sound localization by the Mongolian gerbil, Meriones unguiculatus. J Acoust Soc Am 118:872–886.

Mangin JM, Kunze A, Chittajallu R, Gallo V. 2008. Satellite NG2 progenitor cells share common glutamatergic inputs with associated interneurons in the mouse dentate gyrus. J Neurosci 28:7610–7623.

Mathews PJ, Jercog PE, Rinzel J, Scott LL, Golding NL. 2010. Control of submillisecond synaptic timing in binaural coincidence detectors by K(v)1 channels. Nat Neurosci 13:601–609.

McAlpine D, Jiang D, Palmer AR. 2001. A neural code for low-frequency sound localization in mammals. Nat Neurosci 4:396–401.

Myoga MH, Lehnert S, Leibold C, Felmy F, Grothe B. 2014. Glycinergic inhibition tunes coincidence detection in the auditory brainstem. Nat Commun 5:3790.

Nave KA. 2010. Myelination and support of axonal integrity by glia. Nature 468:244–252.

Overholt EM, Rubel EW, Hyson RL. 1992. A circuit for coding interaural time differences in the chick brainstem. J Neurosci 12:1698–1708.

Pecka M, Brand A, Behrend O, Grothe B. 2008. Interaural time difference processing in the mammalian medial superior olive: the role of glycinergic inhibition. J Neurosci 28:6914–6925.

Pfrieger FW, Slezak M. 2012. Genetic approaches to study glial cells in the rodent brain. Glia 60:681–701.

Roberts MT, Seeman SC, Golding NL. 2013. A mechanistic understanding of the role of feedforward inhibition in the mammalian sound localization circuitry. Neuron 78:923–935.

Salami M, Itami C, Tsumoto T, Kimura F. 2003. Change of conduction velocity by regional myelination yields constant latency irrespective of distance between thalamus and cortex. Proc Natl Acad Sci U S A 100:6174–6179.

Seidl AH. 2014. Regulation of conduction time along axons. Neuroscience 276C:126–134.

Seidl AH, Grothe B. 2005. Development of sound localization mechanisms in the mongolian gerbil is shaped by early acoustic experience. J Neurophysiol 94:1028–1036.

Seidl AH, Rubel EW, Barría A. 2014. Differential conduction velocity regulation in ipsilateral and contralateral collaterals innervating brainstem coincidence detector neurons. J Neurosci 34:4914–4919.

Seidl AH, Rubel EW, Harris DM. 2010. Mechanisms for adjusting interaural time differences to achieve binaural coincidence detection. J Neurosci 30: 70–80.

Smith PH, Joris PX, Yin TC. 1993. Projections of physiologically characterized spherical bushy cell axons from the cochlear nucleus of the cat: Evidence for delay lines to the medial superior olive. J Comp Neurol 331: 245–260.

Sterbing SJ, Hartung K, Hoffmann KP. 2003. Spatial tuning to virtual sounds in the inferior colliculus of the guinea pig. J Neurophysiol 90:2648–2659.

Stevens B, Tanner S, Fields RD. 1998. Control of myelination by specific patterns of neural impulses. J Neurosci 18:9303–9311.

Stotler WA. 1953. An experimental study of the cells and connections of the superior olivary complex of the cat. J Comp Neurol 98:401–431.

Sugihara I, Lang EJ, Llinás R. 1993. Uniform olivocerebellar conduction time underlies Purkinje cell complex spike synchronicity in the rat cerebellum. J Physiol 470:243–271.

Susuki K, Rasband MN. 2008. Molecular mechanisms of node of Ranvier formation. Curr Opin Cell Biol 20:616–623.

Tomassy GS, Berger DR, Chen HH, Kasthuri N, Hayworth KJ, Vercelli A, Seung HS, Lichtman JW, Arlotta P. 2014. Distinct profiles of myelin distribution along single axons of pyramidal neurons in the neocortex. Science 344: 319–324.

van der Heijden M, Lorteije JA, Plauška A, Roberts MT, Golding NL, Borst JG. 2013. Directional hearing by linear summation of binaural inputs at the medial superior olive. Neuron 78:936–948.

Vizoso AD, Young JZ. 1948. Internode length and fibre diameter in developing and regenerating nerves. J Anat 82:110–134.1.

de Waegh SM, Lee VM, Brady ST. 1992. Local modulation of neurofilament phosphorylation, axonal caliber, and slow axonal transport by myelinating Schwann cells. Cell 68:451–463.

Wake H, Lee PR, Fields RD. 2011. Control of local protein synthesis and initial events in myelination by action potentials. Science 333:1647–1651.

Walsh EJ, McGee J. 1988. Rhythmic discharge properties of caudal cochlear nucleus neurons during postnatal development in cats. Hear Res 36:233–247.

Waxman SG. 1971. An ultrastructural study of the pattern of myelination of preterminal fibers in teleost oculomotor nuclei, electromotor nuclei, and spinal cord. Brain Res 27:189–201.

Waxman SG. 1975. Integrative properties and design principles of axons. Int Rev Neurobiol 18:1–40.

Waxman SG, Melker RJ. 1971. Closely spaced nodes of Ranvier in the mammalian brain. Brain Res 32:445–448.

Waxman SG, Sims TJ. 1984. Specificity in central myelination: Evidence for local regulation of myelin thickness. Brain Res 292:179–185.

Werthat F, Alexandrova O, Grothe B, Koch U. 2008. Experience-dependent refinement of the inhibitory axons projecting to the medial superior olive. Dev Neurobiol 68:1454–1462.

Wilkinson F. 1986. Eye and brain growth in the Mongolian gerbil (Meriones unguiculatus). Behav Brain Res 19:59–69.

Woolf NK, Ryan AF. 1984. The development of auditory function in the cochlea of the mongolian gerbil. Hear Res 13:277–283.

Yin TC, Chan JC. 1990. Interaural time sensitivity in medial superior olive of cat. J Neurophysiol 64:465–488.

Young SR, Rubel EW. 1983. Frequency-specific projections of individual neurons in chick brainstem auditory nuclei. J Neurosci 3:1373–1378.

Ziskin JL, Nishiyama A, Rubio M, Fukaya M, Bergles DE. 2007. Vesicular release of glutamate from unmyelinated axons in white matter. Nat Neurosci 10:321–330.